INTERNATIONAL JOURNAL FOR NUMERICAL METHODS IN FLUIDS, VOL. 4, 765–780 (1984)

ON THE INTERACTIONS OF SURFACE WAVES WITH IMMERSED STRUCTURES

H. W. K. BIRD

Associate Engineer, SF/Braun, Orange, California 92668, U.S.A.

R. SHEPHERD

Professor of Civil Engineering, University of California Irvine, California 92717, U.S.A.

SUMMARY

The fluid forces resulting from wave interaction with large submerged structures may be calculated using numerical procedures based on the solution of the associated boundary-value problem. In this paper, the analysis of wave interaction with a fixed submerged object of arbitrary cross-section and infinite length using a two-dimensional boundary value formation based on linear diffraction theory is summarized. Subsequently, the application of the boundary element method to obtain a solution is presented. The numerical considerations are emphasized with particular reference to computational efficiency.

Numerical results are presented in the form of dimensionless wave force plots for various structural shapes. In the case of a bottom-seated half cylinder, for which there exists a closed-form solution, comparisons are made between results generated using both boundary element and equivalent finite element approaches. In the case of a submerged cylinder, comparisons are made between boundary element derived values and experimental results. The boundary element results compare well with both the closed-form solution and the experimental values.

KEY WORDS Diffraction Hydrodynamics Ocean Engineering Underwater Structures Wave Forces Offshore Structures Velocity Potential Boundary Elements

INTRODUCTION

The analysis of the interaction of surface waves with an immersed structure necessitates the consideration of diffraction effects when the structure size is large relative to the incident wave length. Examples of such structures are concrete gravity platforms and submerged oil storage tanks. The role of the diffraction phenomenon in the determination of fluid loadings on large diameter offshore structures has been outlined in a state of the art appraisal of fluid loadings.[1]

Problems in which diffraction of the incident wave must be accounted for have been tackled in a variety of ways. The use of functional diffraction coefficients (as functions of the frequency or wavelength) has been suggested.[2] The application of Stokes' non-linear wave theory to a bottom-seated, deeply submerged half cylinder and hemisphere, has led to the development of approximate closed form solutions for the wave forces.[3] Closed form solutions for diffraction around piles[4] and submerged cylindrical tanks[5] have been proposed.

These approaches to the solution of diffraction problems are low cost with respect to development and computer time, but are restricted in their application to objects of simple

0271–2091/84/080765–16$01.60

Received 28 April 1983
Revised 28 July 1983

geometry. A more general type of solution is provided by diffraction theory. Applications of diffraction theory in the form of direct numerical solution of the associated boundary-value problem, have in recent years been made more practical with increases in the memory size and computing speed of digital computers.

In diffraction theory a solution to the problem of wave–structure interaction is set up in terms of a velocity potential. Diffraction theory is normally applied in a linearized form. The formulation is that of a boundary-value problem governed by Laplace's equation and having mixed boundary conditions. A linearized free surface boundary condition, the kinematic boundary conditions on the surface of the structure and on the sea floor, and a distant radiation condition for the diffracted wave must all be satisfied.

The boundary-value problem described above may be solved numerically in several ways. The Green's function method[6] is one that has been used extensively. Sources are distributed over the surface of the object, an integral equation for the potential over the boundary of the object is then developed, a Green's function being used to represent the source potential. Several applications of this method have been reported.[7–10]

Finite element methods also may be used to solve the boundary-value problems associated with wave–structure interaction. One approach involves using a variational principle to determine the velocity potential throughout the fluid domain.[11,12]

In this paper Green's second identity and a fundamental solution[13–16] are used to develop a boundary integral equation over the full boundary of the problem domain and this leads to the development of a two-dimensional numerical solution to the boundary-value problem. This approach has recently been extended to the three-dimensional domain[7,18] and to solutions using a non-linear incident wave.[19] The fundamental solution is simple in form and only satisfies the domain condition. This is in contrast to the Green's function method where the derivation of the Green's function that satisfies all or some of the imposed boundary conditions is generally difficult and sometimes impossible. The resulting boundary integral equation is solved approximately by dividing the full boundary of the domain into elements and numerically integrating over each element in turn. Systematic application of the boundary integral to each element nodal point yields a set of simultaneous equations which are solved to obtain nodal values for the diffracted-wave potential. The wave forces and pressures on the structure are calculated from the velocity potential of the wave. Several objects of symmetry are used in presenting the results of the analyses.

THEORY

Formulation of the boundary-value problem

The formulation of the problem set up within the framework of two-dimensional linear diffraction theory, has been stated previously[20] but is presented here in a summary form for completeness (equations (1)–(9)). Under the assumptions of potential flow, small wave amplitude, and a direction of wave propagation that is normal to the longitudinal axis of the object a linearized harmonic velocity potential $\Phi(x, y, t)$ is introduced as the real part of a complex function in the form

$$\Phi(x, y, t) = \mathrm{Re}\,[\phi(x, y)e^{-i\sigma t}] \tag{1}$$

where $\phi(x, y)$ is the spatial velocity potential and σ is the incident wave frequency such that $\sigma = 2\pi/T$ in which T is the period of motion.

The fluid is bounded by an impermeable bottom boundary at $y = -d$ and a mean free

surface at $y = 0$ (see Figure 1). The spatial velocity potential $\phi(x, y)$ satisfies the Laplace equation within the fluid domain and is subject to a linearized mixed type boundary condition on the mean free surface, and kinematic boundary conditions on the ocean bottom and the surface of the object.

Decomposition of the spatial velocity potential into incident and diffracted components enables a boundary-value problem for the diffracted potential $\phi_D(x, y)$ to be written as

$$\text{Laplace's equation} \quad \nabla^2\phi_D(x, y) = 0 \quad \text{in } \Omega \tag{2a}$$

$$\text{Object surface} \quad \frac{\partial\phi_D}{\partial n} = -\frac{\partial\phi_I}{\partial n} \quad \text{on } \Gamma_1 \tag{2b}$$

$$\text{Ocean bottom} \quad \frac{\partial\phi_D}{\partial n} = 0 \quad \text{on } \Gamma_2 \tag{2c}$$

$$\text{Radiation boundary} \quad \frac{\partial\phi_D}{\partial n} - ik\phi_D = 0 \quad \text{on } \Gamma_3(x \pm x_r) \tag{2d}$$

$$\text{Free surface} \quad \frac{\partial\phi_D}{\partial n} - k_0\phi_D = 0 \quad \text{on } \Gamma_4 \tag{2e}$$

where k_0 is defined by the dispersion relation

$$k_0 = k \tanh kd = \frac{\sigma^2}{g} \tag{3}$$

in which d is the ocean depth, g is the acceleration due to gravity and k is a wave number. From linear wave theory, the incident potential $\phi_I(x, y)$ corresponding to a train of right-running waves is given in complex form as

$$\phi_I(x, y) = \frac{-iga_0 \cosh[k(d + y)]}{\sigma \cosh[kd]} e^{ikx} \tag{4}$$

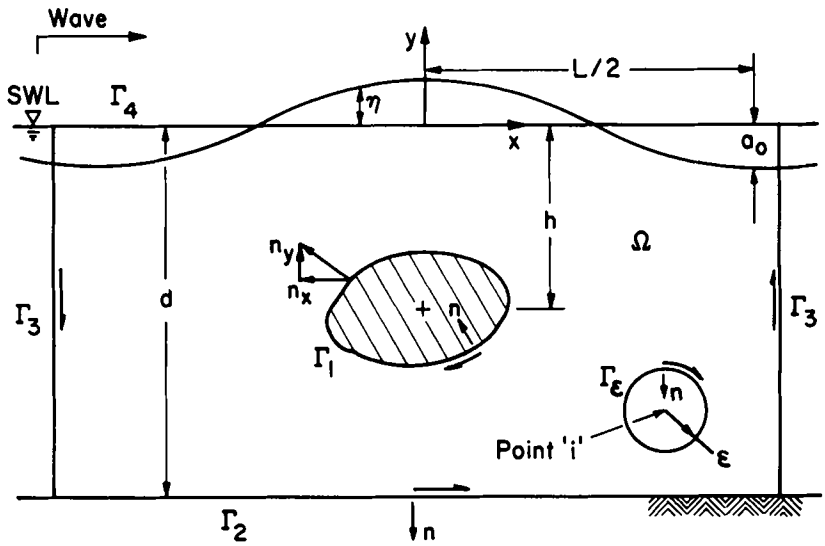

Figure 1. Definition sketch

where a_0 is the wave amplitude. The incident potential derivative, $-\partial\phi_I/\partial n$, in equation 2(b), is equivalent to the incident wave velocity $v_n(x, y)$ which is represented in complex form by

$$v_n(x, y) = -\frac{ga_0k}{\sigma}\left\{n_x\frac{\cosh[k(d+y)]}{\cosh[kd]} + in_y\frac{\sinh[k(d+y)]}{\cosh[kd]}\right\}e^{ikx} \tag{5}$$

where n_x and n_y are components of the outward unit normal vector on the surface of the object in the x and y directions, respectively. Equation 2(d) represents a radiation condition that the diffracted potential must satisfy at large distances from the object such that only outgoing waves are admitted. For modelling purposes it is assumed that the local disturbance at the object decays sufficiently at a finite distance, x_r, from the object to justify the radiation condition being applied on a truncated boundary at $x = x_r$.

The boundary integral equation

In order to solve the boundary-value problem described by equation (2a)–(2e) an approximation for the diffracted-wave potential ϕ_D is introduced which is represented by the complex potential function ϕ. A source function, u^*, known as the fundamental solution, is introduced and Green's second identity is applied to the pair of functions, ϕ and u^*, to obtain an integral equation on the full boundary of the domain. The fundamental solution for a two-dimensional isotropic medium is given by the expression

$$u^* = \frac{1}{2\pi}\ln\left(\frac{1}{r}\right) \tag{6}$$

where r is the distance between the observation point and the 'source' point i. This solution satisfies the domain condition of the problem, but does not satisfy any of the boundary conditions.

A general boundary solution for the unknown function ϕ, formulated for a point i lying anywhere along the boundary is written as

$$c_i\phi_i + \int_{\Gamma_1+\Gamma_2}\frac{\partial u^*}{\partial n}\phi\,d\Gamma + \int_{\Gamma_3}\left(\frac{\partial u^*}{\partial n} - iku^*\right)\phi\,d\Gamma + \int_{\Gamma_4}\left(\frac{\partial u^*}{\partial n} - k_0u^*\right)\phi\,d\Gamma = \int_{\Gamma_1}u^*q\,d\Gamma \tag{7}$$

where q is the normal derivative of the potential function ϕ and $c_i = 1/2$ for smooth boundaries but, in general, will depend on the form of the boundary on which the point i is located.

A solution for the function ϕ is found by applying equation (7) numerically at each nodal point, i, on the boundary of the domain, thus building up a matrix system of equations. Nodal values of the function ϕ, the diffracted-wave potential, then may be obtained by solving the system of equations.

Wave pressure and forces

Once nodal values of the diffracted-wave potential have been obtained, the total spatial velocity potential $\phi(x, y)$ is found by summing the diffracted and incident components.

The dynamic pressure $P(x, y, t)$ on the structure is found from the velocity potential by using the linearized Bernoulli equation given as

$$P(x, y, t) = -\rho\frac{\partial\Phi}{\partial t} = \mathrm{Re}\left[i\rho\sigma\phi(x, y)e^{-i\sigma t}\right] \tag{8}$$

where ρ is the density of the fluid.

The wave forces are found by integrating the dynamic pressure over the surface of the object. The force per unit length of the object is calculated in component form as

$$F_x = -\int_{\Gamma_1} P(x, y, t)\,dy \quad \text{and} \quad F_y = \int_{\Gamma_1} P(x, y, t)\,dx \tag{9}$$

NUMERICAL SOLUTION

Matrix formulation

In general the boundary integral equation developed in the preceding paragraphs may be solved only approximately by using numerical techniques. The solution method consists of using discrete elements to model the full boundary of the domain. Equation (7) is written in discretized form for n boundary elements as

$$c_i\phi_i + \sum_{n_1+n_2}\int_{\Gamma_j}\phi_j\frac{\partial u^*}{\partial n}\,d\Gamma + \sum_{n_3}\int_{\Gamma_j}\phi_j\left(\frac{\partial u^*}{\partial n} - iku^*\right)d\Gamma + \sum_{n_4}\int_{\Gamma_j}\phi_j\left(\frac{\partial u^*}{\partial n} - k_0u^*\right)d\Gamma = \sum_{n_1}\int_{\Gamma_j} q_ju^*\,d\Gamma \tag{10}$$

where n_k refers to the elements on boundary Γ_k. Either elements with a linear or quadratic (see Figures 2 and 3) variation of ϕ and q along their length are used to model the boundary. For linear elements the integral terms in equation (10) may be written in terms of linear interpolation functions ψ_1 and ψ_2 as

$$\int_{\Gamma_j}\phi_j\frac{\partial u^*}{\partial n}\,d\Gamma = \int_{\Gamma_j}[\psi_1\ \psi_2]\frac{\partial u^*}{\partial n}\,d\Gamma\begin{Bmatrix}\phi_1\\ \phi_2\end{Bmatrix} = [h_{j1}\ h_{j2}]\begin{Bmatrix}\phi_1\\ \phi_2\end{Bmatrix} \tag{11a}$$

and

$$\int_{\Gamma_j}\phi_ju^*\,d\Gamma = \int_{\Gamma_j}[\psi_1\ \psi_2]u^*\,d\Gamma\begin{Bmatrix}\phi_1\\ \phi_2\end{Bmatrix} = [g_{j1}\ g_{j2}]\begin{Bmatrix}\phi_1\\ \phi_2\end{Bmatrix} \tag{11b}$$

where ϕ_1 and ϕ_2 are nodal values.

Writing equation 10 for each nodal point i in turn yields a full set of equations for a nodes which may be expressed in matrix form as

$$\mathbf{A}\boldsymbol{\phi} = \mathbf{F} \tag{12}$$

where $\mathbf{A}$ is a complex fully populated n by n matrix. $\boldsymbol{\phi}$ is the complex vector of unknown

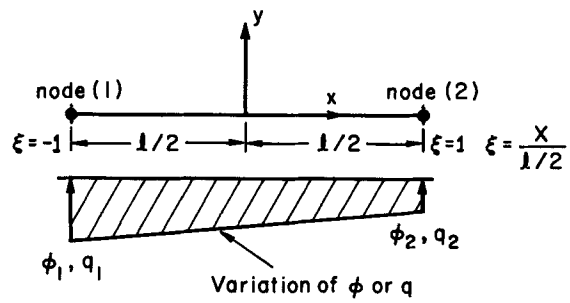

Figure 2. Linear element

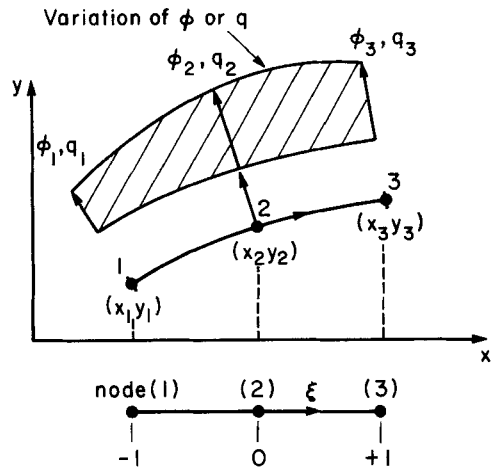

Figure 3. Quadratic element

nodal diffracted potentials, and **F** is a complex vector of nodal terms of which only those corresponding to the nodes on the surface of the object will be non-zero.

Solution steps

The steps that lead to the final solution of the boundary-value problem and the subsequent generation of wave forces are shown in Figure 4. These steps form the basis of linear element and quadratic element FORTRAN codes that have been written for a PDP 11/34A computer.

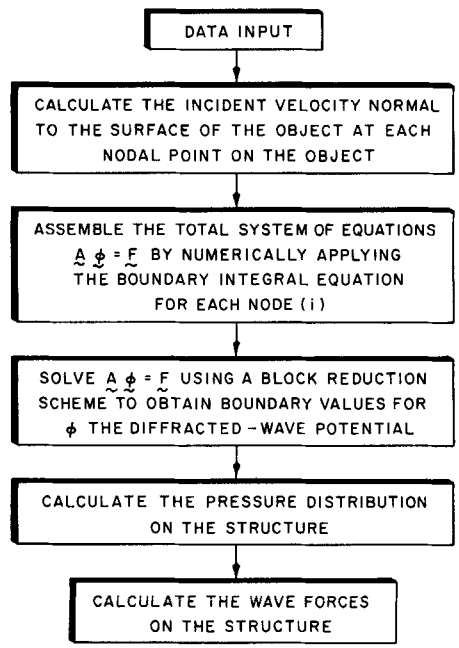

Figure 4. Solution steps

The amount of input data required for these boundary element programs is relatively small compared to that of equivalent finite element formulations. This is evident from Figure 7 where boundary element and finite element models are shown for a bottom-seated half-cylinder. The boundary element input data consists of boundary node co-ordinates and various problem parameters. An equivalent finite element model would additionally require the input of internal node co-ordinates and element connectivities.

Owing to the relatively small amount of core memory available on the PDP 11/34A computer, the full system matrix **A** and vector **F** are stored on disk in a series of blocks. The incident velocity normal to the surface of the object is calculated using equation (5) at each nodal point on the object. The full system of equations is then assembled by applying equation (10) at each nodal point i in turn. The nodal terms in matrix **A** are calculated by summing the element contributions of the integral terms in equations (11a) and (11b). The calculation of these integral terms, which in general is carried out using numerical integration, is discussed in a later section of this paper.

The assembled system of equations (12) is solved using the block reduction scheme shown in Figure 5. Each block of equations is in turn read into the main core memory, reduced using Gaussian row elimination, then written back into disk. The blocks of equations are read and written in an unformatted sequential format which saves execution time by eliminating the data conversion process.

The solution of the system of equations represents nodal values for the diffracted wave potential. Combining the incident and diffracted potentials together enables the pressure and

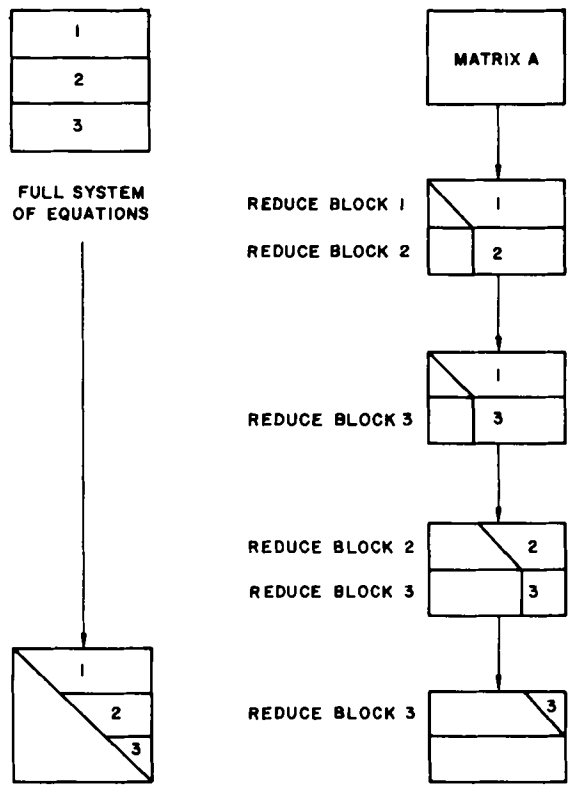

Figure 5. Block reduction scheme for the system of equations

fluid forces resulting from the wave–structural interaction to be calculated using equations (8) and (9), respectively.

Numerical integration

The integral terms,

$$\int_{\Gamma_j} \phi_i \frac{\partial u^*}{\partial n} \mathrm{d}\Gamma \quad \text{and} \quad \int_{\Gamma_j} \phi_j u^* \mathrm{d}\Gamma$$

are in general evaluated using numerical integration techniques. The case of a linear element discretization is considered below.

For all elements that do not include the node under consideration, the integral components, h_{il} $l = 1, 2$ and, g_{jl} $l = 1, 2$, in equations (11a) and (11b), are calculated using a 4-point Gauss quadrature rule as follows:

$$h_{jl} = \sum_{k=1}^{4} -\frac{1}{2\pi} \frac{\mathrm{DIST}}{\mathrm{RA}(\xi_k)} \frac{\psi_l(\xi_k)}{\mathrm{RA}(\xi_k)} w_k \frac{[(X1-X2)^2+(Y1-Y2)^2]^{1/2}}{2} \quad \text{for} \quad l = 1, 2 \qquad (13a)$$

$$g_{jl} = \sum_{k=1}^{4} -\frac{1}{2\pi} \ln\left[\frac{1}{\mathrm{RA}(\xi_k)}\right] \psi_l(\xi_k) w_k \frac{[(X1-X2)^2+(Y1-Y2)^2]^{1/2}}{2} \quad \text{for} \quad l = 1, 2 \qquad (13b)$$

where $\psi_l(\xi_k)$ is the interpolation function, w_k $k = 1, 2, 3, 4$ are the four weights, ξ_k $k = 1, 2, 3, 4$ are the four integration points and X and Y are the co-ordinates of the extreme points of the element j. The variables $\mathrm{RA}(\xi_k)$ and DIST are as shown in Figure 6.

When the element to be integrated includes the node under consideration, the components h_{j1} and h_{j2} are zero, owing to the orthogonality of the normal vector and the vector between

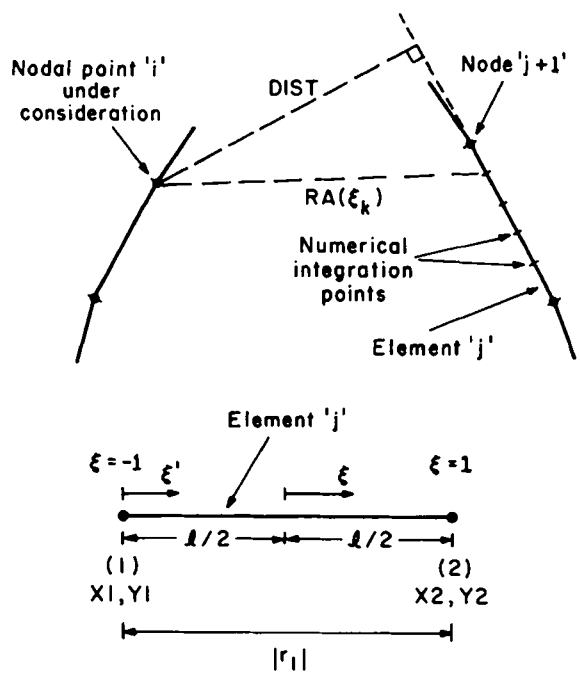

Figure 6. Numerical integration scheme for linear elements

the source and integration points (see equation (11a)) the components g_{j1} and g_{j2}, however, are calculated using the following analytical expressions

$$g_{j1} = \frac{|r_1|}{2\pi}\left(0{\cdot}5 \ln \frac{1}{|r_1|} + 0{\cdot}75\right) \tag{14a}$$

and

$$g_{j2} = \frac{|r_1|}{2\pi}\left(0{\cdot}5 \ln \frac{1}{|r_1|} + 0{\cdot}25\right) \tag{14b}$$

where r_1 is the length of the element. These expressions are developed by substituting the fundamental solution given by equation (6) into equation (11b) and carrying out the integration.

In the case of quadratic elements the integral components are computed using an 8-point Gauss quadrature rule for all elements that do not include the node under consideration. The integral components for a quadratic element which includes the node under consideration cannot be calculated analytically as with linear elements, owing to the complexity of the integration. Hence, the h_{ji} terms, which are not generally zero, are calculated using 8-point Gauss quadrature. The g_{j1} terms are calculated using a logarithmically weighted numerical integration formula that takes into account the asymtopic behaviour of the fundamental solution near the source point i. For a more detailed discussion of these numerical integration techniques the reader is referred to References 20 and 21.

Modelling considerations

The accuracy of the results generated using this numerical procedure is dependent on the boundary element discretization that is used to model a particular problem. Good convergence is generally obtained using less than 100 nodal points distributed around the full

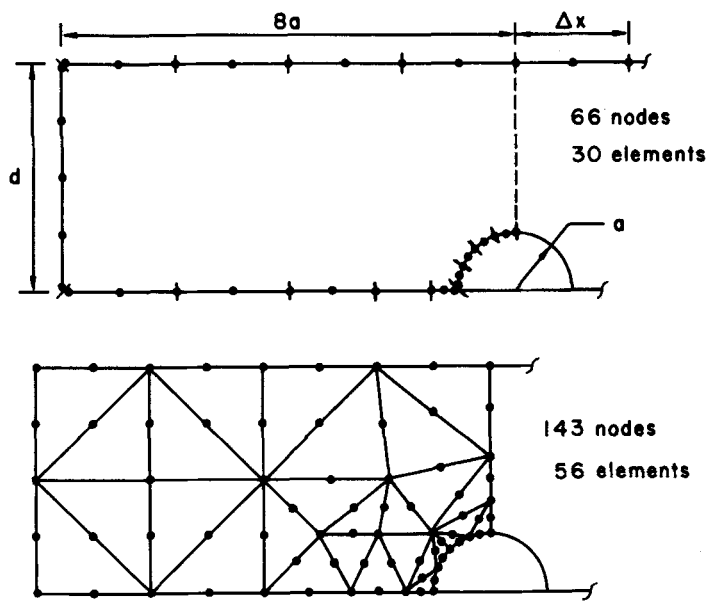

Figure 7. Discretizations for a bottom-seated half cylinder with $d/a = 4.0$

boundary. The following consideration, however, should be noted when deciding upon the discretization for a model.

Where nodal points are positioned at changes in direction of the object boundary it may be necessary to define two nodes in order to bridge the discontinuity in the normal velocity profile. In the case of a linear boundary element model, double nodes are defined for all nodal points that are positioned at changes in direction of the object boundary. An example of this is shown in Figure 7 for curved quadratic elements, where double nodes are only defined for nodal points positioned at sharp changes in direction of the object boundary.

The number of elements required to model the free surface boundary increases as the wavelength decreases (or k increases). A linear element length, Δx, equal to or less than one-eight of the incident wave length is found to be adequate. Also if the object is positioned close to the free surface or the ocean floor, more elements are required to model those respective boundaries and the object boundary because of the singular behaviour of the fundamental solution near the boundary.

The modelling and truncation of the radiation boundary has less of a bearing on the numerical results than the discretization of the other boundaries. The allowable truncation distance x_r will depend on the degree of diffraction of the incident wave by the object. In general, x_r should be increased as the relative depth d/a, or relative submergence h/a decrease, and the relative wavelength $2\pi a/L$ increases. For most problems, a truncation distance of five object diameters is sufficient.

RESULTS AND DISCUSSION

The wave interactions with a bottom-seated horizontal half cylinder, a submerged horizontal cylinder and a submerged rectangular block are analysed. For the half cylinder, a classical solution exists. This classical solution[20,22] is used to test the convergence of a quadratic boundary element model which is compared to that of an equivalent six-node finite element model. Boundary element results for the submerged horizontal cylinder are compared to experimental data.

Results for the half-cylinder and cylinder are presented in the form of dimensionless wave force plots. In addition, pressure distributions on the surface of the object are presented for all three objects.

CONVERGENCE TEST

Three different sets of quadratic boundary element and six-node finite element discretizations are used to model a bottom seated horizontal half cylinder. The finest pair of these meshes is shown in Figure 7.

Figures 8–11 show the dimensionless horizontal and vertical wave forces, $f_x = F_{x\max}/(\rho g a a_0)$ and $f_y = F_{y\max}/(\rho g a a_0)$ plotted against the dimensionless wave number, ka, for the depth-to-radius ratio d/a equal to 4.0. The horizontal force plots show that the boundary element models have obtained a better degree of convergence than the equivalent finite element models. The horizontal forces have not converged fully to the asymptotic solution because the numerical models take into account the effect of the free surface on the diffracted wave where as the asymptotic solution neglects this effect.

The vertical force plots show very good convergence for both the boundary element and the finite element models. This is because the vertical forces on a half cylinder are more dependent on the incident potential than the calculated diffracted potential.

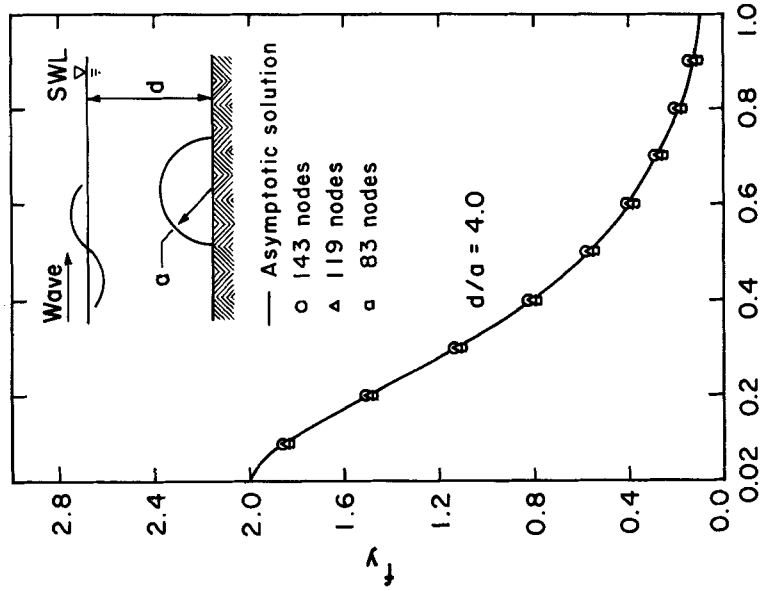

Figure 9. Quadratic boundary element convergence—vertical wave forces

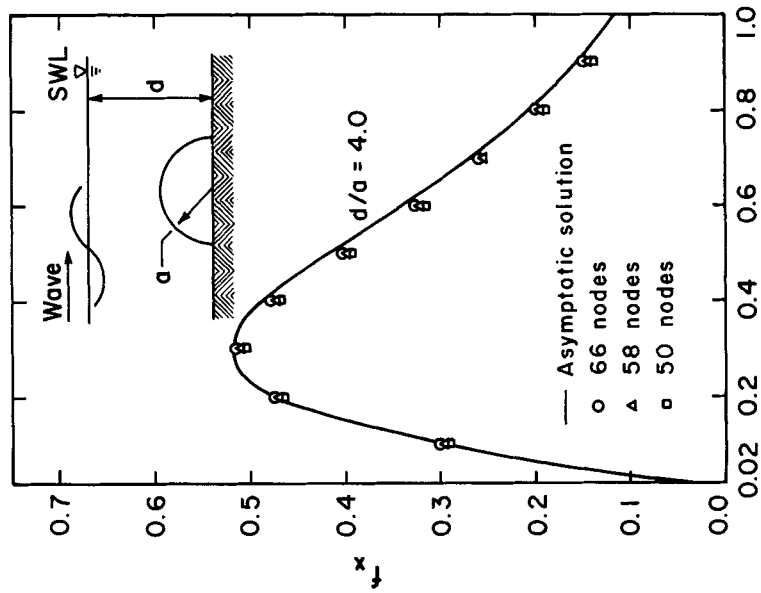

Figure 8. Quadratic boundary element convergence—horizontal wave forces

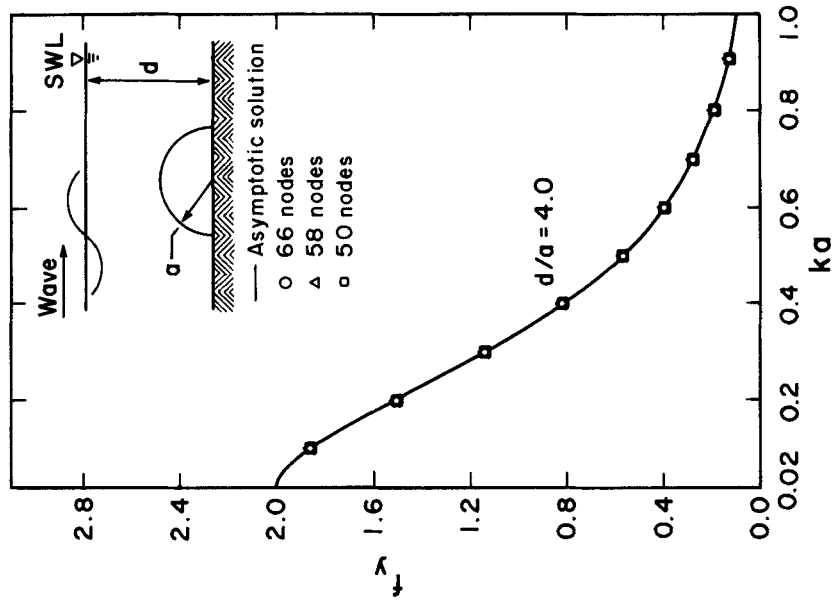

Figure 11. Six-node finite element convergence—vertical wave forces

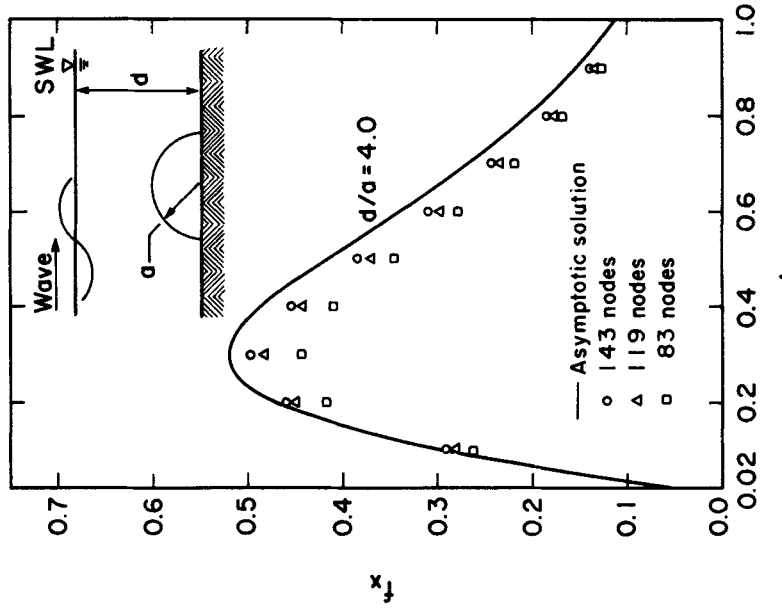

Figure 10. Six-node finite element convergence—horizontal forces

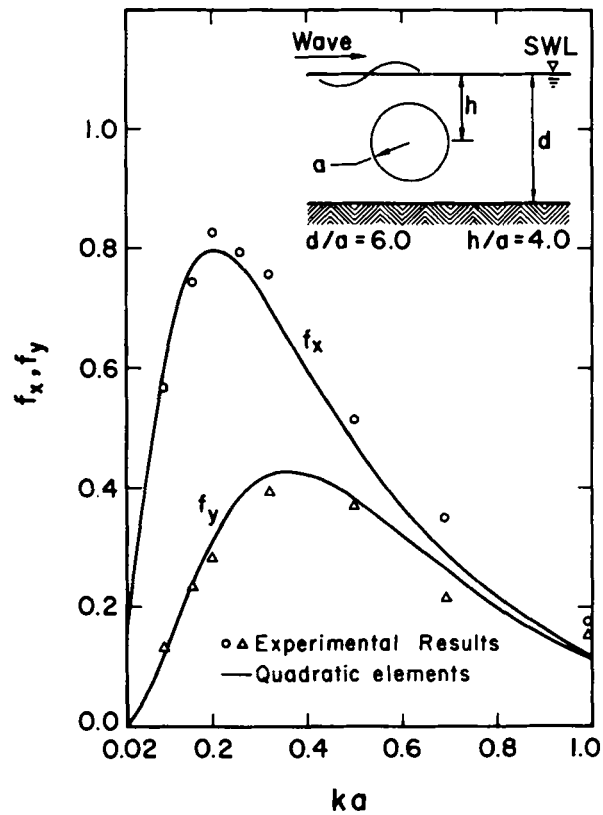

Figure 12. Horizontal and vertical wave forces on a submerged horizontal cylinder

SUBMERGED HORIZONTAL CYLINDER

Model tests on a cylindrical tank of radius 6 in. as shown in Figure 12 have been carried out.[23] In the series of analyses considered here, the cylinder was suspended in the tank from the top such that $h/a = 4{\cdot}0$ and the depth of water was such that $d/a = 6{\cdot}0$.

Figure 12 shows the dimensionless wave forces f_x and f_y plotted against ka. The agreement between the experimental results and the numerical curves is good. It is noted that this agreement improves as ka decreases, where ka may be interpreted as the dimensionless wave steepness $2a_0/L$.

PRESSURE DISTRIBUTION

The pressure distribution resulting from wave interaction with a submerged object obtained for the cases of a half cylinder, a cylinder and a rectangular block is shown in Figures 13 and 14. The pressures are calculated in the dimensionless form $p(x, y, t) = P(x, y, t)/(\rho g a_0)$ and the distributions around the objects are plotted diagrammatically at four different times within one wave period for the wave number $k = 0{\cdot}05$.

When placed in shallow water with $d/a = 2{\cdot}5$, as shown in Figure 13, the objects cause a noticeable blocking, or diffraction, of the flow resulting in a higher pressure at the front of the object than at the back. This is well illustrated for the case of the cylinder (see Figure 13(b)).

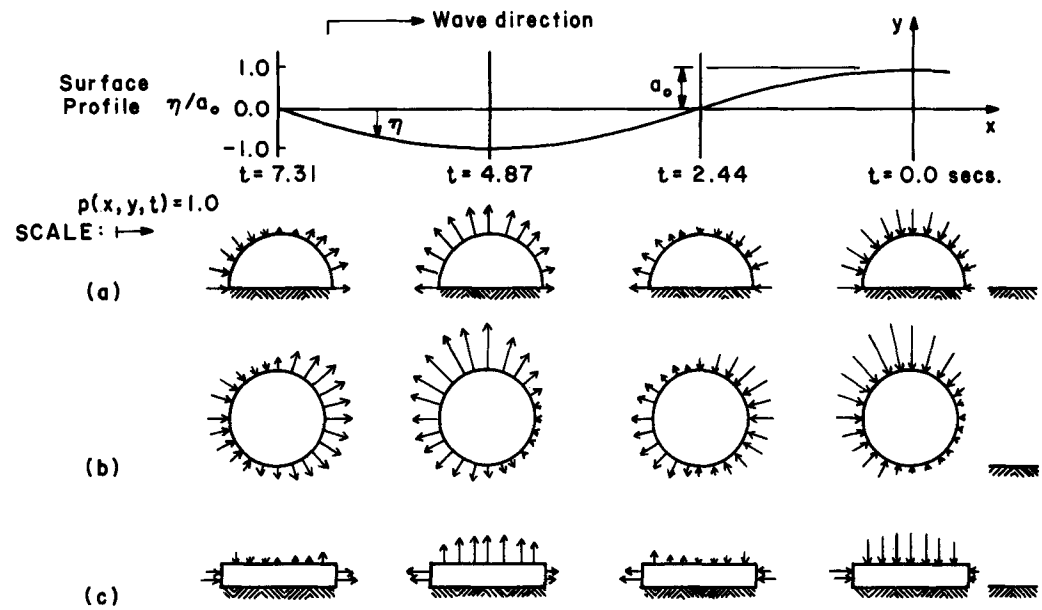

Figure 13. Pressure distribution on submerged objects for $d/a = 2{\cdot}5$

In Figure 14 the objects are shown positioned in deeper water with $d/a = 6{\cdot}0$. For this case there is very little blocking of the flow, so producing a more balanced pressure distribution and smaller magnitudes of pressure.

Considering the pressure distributions for both values of d/a at each time step it is noted that the pressure variation is mainly dependent upon the position of the incident wave profile relative to that of the object. As the value of d/a decreases however, the diffraction of the

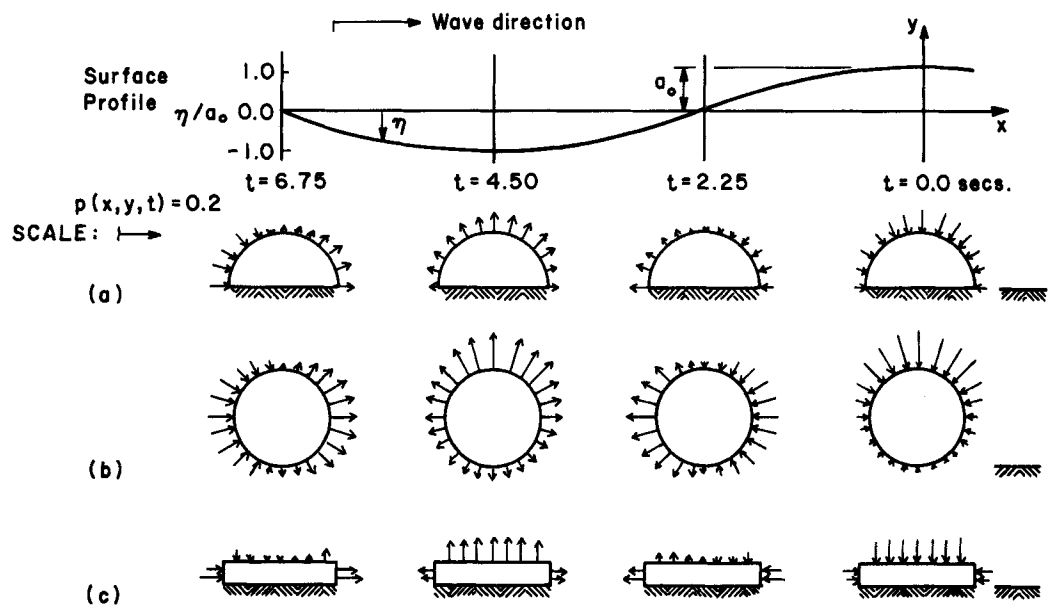

Figure 14. Pressure distribution on submerged objects for $d/a = 6{\cdot}0$

incident wave becomes more important and will have a large effect on the pressure distribution around an object.

CONCLUSIONS

The numerical technique presented above is shown, for the several objects that are analysed, to give results that compare well with known solutions and experimental data. The efficiency of the technique is demonstrated by the good convergence that is obtained while using relatively few elements to model the boundary of the problem.

ACKNOWLEDGEMENTS

The work described was undertaken by the first author as part of his graduate studies under the supervision of the second author. The project was initiated by Dr. Carols A. Brebbia, sometime Professor of Civil Engineering at the University of California, Irvine. The contributon of Dr. Brebbia and of Dr. Friedel Hartmann, visiting Research Fellow at UCI, is recorded with gratitude.

REFERENCES

1. N. Hogben, 'Fluid loading on offshore structures. A state-of-art appraisal-wave loads', *National Physical Laboratory Ship*, T. M. 381, Teddington, February, 1974.
2. N. G. Hogben, and R. G. Standing, 'Experience in computing wave loads on large bodies', *Proc. Offshore Technology Conf.*, OTC 2189, Houston, 1975.
3. S. K. Chakrabarti and R. A. Naftzger, 'Nonlinear wave forces on half cylinder and hemisphere', *Journal of the Waterways, Harbors and Coastal Engineering Division, ASCE*, **100,** (WW3), *Proc. Paper* 10710, August, 189–204 (1974).
4. R. C. MacCamy and R. A. Fuchs, 'Wave forces on piles—a diffraction theory', *Beach Erosion Board Technical Memorandum No.* 69, U.S. Army Corps of Engineers, 1954.
5. S. Gran, 'Wave forces on submerged cylinders', *Proc. Offshore Technology Conf.*, OTC 1817, Houston, 1973.
6. F. John, 'On the motion of floating bodies II', *Communication in Pure and Applied Mathematics*, **3,** 45–101 (1950).
7. C. J. Garrison, 'Hydrodynamic loading of large offshore structures: three-dimensional source distribution methods' in *Numerical Methods in Offshore Structures*, O. C. Zienkiewwicz, R. W. Lewis, K. G. Stagg (eds), 1st edn., Wiley, Chichester, 1978.
8. C. J. Garrision and P. Y. Chow, 'Wave forces on submerged bodies', *Journal of the Waterways, Harbors and Coastal Engineering Division, ASCE*, **98,** (WW2), *Proc. Paper* 9098, August, 375–392 (1972).
9. C. J. Garrison and V. S. Rao, 'Interaction of waves with submerged objects', *Journal of the Waterways, Harbors and Coastal Engineering Division, ASCE*, **97,** (WW2), *Proc. Paper* 8111, May, 259–278 (1971).
10. R. A. Naftzger and S. K. Chakrabarti, 'Scattering of Waves by Two-dimensional circular objects in finite water depths', *Journal of Ship Research*, **23,** (1), 32–42 (1979).
11. K. J. Bai, 'Diffusion of oblique waves by an infinite cylinder', *Journal of Fluid Mechanics*, **68,** Part 3, 513–535 (1975).
12. S. Vongvissessomjai and M. Hanif, 'Wave forces on elliptical cylinders by finite element methods', *Proceedings of the First International Conference on Envirionmental Forces on Engineering Structures*, Imperial College, London, England, July, 1979, pp. 219–235.
13. K. J. Bai and R. W. Yeung, 'Numerical solutions to free surface flow problems', *Proceedings, Tenth Naval Hydrodynamics Symposium*, M.I.T., Cambridge, Mass., June, 1974, pp 609–647.
14. P. K. Banerjee and R. P. Shaw, (Eds) *Developments in Boundary Element Methods*—2, Applied Science Publishers Ltd., 1982.
15. C. A. Brebbia, *The Boundary Element Method for Engineers*, Pentech Press, London, England, 1978.
16. R. W. Yeung, 'A hybrid integral equation method for time-harmonic free surface flow', *Proceedings, First International Conference on Numerical Ship Hydrodynamics*, David Taylor Naval Ship Research and Development Center, 1975, pp. 581–607.
17. M. C. Au and C. A. Brebbia, 'Diffraction of water waves for vertical cylinders using boundary elements', *Applied Mathematical Modelling*, **7,** (2), 106–118 (1983).
18. M. C. Au and C. A. Brebbia, 'Numerical prediction of wave forces using the boundary element method', *Applied Mathematical Modelling*, **6,** (4), 218–228 (1982).
19. M. de St. Q. Isaacson, 'Nonlinear—wave effects on fixed and floating bodies', *Journal of Fluid Mechanics*, **120,** 267–281 (1982).

20. H. W. K. Bird, 'Wave interaction with large submerged structures—a two-dimensional boundary element approach', *MSc. thesis* University of California at Irvine, California, 1981.
21. A. H. Stroud and D. Secrest, 'Gaussian quadrature formulae', Prentice-Hall, New York, 1949.
22. H. W. K. Bird and R. Shepherd, 'Wave interaction with large submerged structures', *Journal of the Waterway, Port, Coastal and Ocean Division, ASCE,* **108,** (WW2), Proc. Paper 17103, May, 146–162 (1982).
23. F. C. Schiller, 'Wave forces on a submerged horiziontal cylinder', *Master's Thesis,* Naval Postgraduate School, Monterey, California, Report No. AD 727 691, June, 1971, 99 pp.